Improved Carbon Corrosion and Platinum Dissolution Durability in Automotive Fuel Cell Startup and Shutdown Operation

Journal of The Electrochemical Society, 2021 **168** 034503

Improved Carbon Corrosion and Platinum Dissolution Durability in Automotive Fuel Cell Startup and Shutdown Operation

Chunmei Wang,[1,†] Mark Ricketts,[1] Amir Peyman Soleymani,[2,3] Jasna Jankovic,[2,3,*] James Waldecker,[1] Jixin Chen,[1,z] and Chunchuan Xu[1]

[1]*Ford Motor Company, Dearborn, Michigan 48121, United States of America*
[2]*Center for Clean Energy Engineering, Institute of Materials Science, University of Connecticut, Storrs, Connecticut, 06269, United States of America*
[3]*Department of Materials Science and Engineering, University of Connecticut, Storrs, Connecticut, 06269, United States of America*

Three protocols of accelerated startup and shutdown (SU/SD) test were investigated: startup and shutdown with air supply and soak to both anode and cathode (air-SU/SD), hydrogen protected startup and shutdown (H_2-SU/SD), and hydrogen protected startup and shutdown with a load (H_2-SU/SD with a load). The performance losses, electrochemical surface area (ECSA) reduction, and catalyst layer degradation were characterized and compared for these SU/SD protocols. Air-SU/SD protocol showed much more severe performance loss and catalyst layer degradation than hydrogen protected ones, which confirmed the benefits of hydrogen protection. The temperature effect on air-SU/SD was significant in a broad range from 20 °C to 70 °C, with low temperature greatly reducing the degradation. The mechanism of H_2 protection and load drawn in alleviating carbon corrosion was explained based on reactions and charge conservation during SU/SD. This paper provides comprehensive test data and failure analysis to quantify the benefits of H_2 protection and load drawn and to facilitate future enhancement of system strategies on SU/SD durability.
 [DOI: 10.1149/1945-7111/abe6ea]

Manuscript submitted December 14, 2020; revised manuscript received February 3, 2021. Published March 1, 2021. *This paper is part of the JES Focus Issue on Proton Exchange Membrane Fuel Cell and Proton Exchange Membrane Water Electrolyzer Durability.*

Automotive polymer electrolyte membrane (PEM) fuel cell (FC) has been increasingly under development, due to its ability to provide extended driving ranges at zero emission. However, PEM fuel cells still face several challenges, such as durability and cost. The lifetime of a PEM fuel cell stack is determined by the durability of key component materials, including catalyst, membrane and ionomer that are exposed to strongly acidic and oxidizing conditions in a fuel cell. The durability of stack materials is affected by various operating modes and hydration conditions during drive cycles, idling conditions and startup/shutdown (SU/SD) cycles.[1] From a 2019 European Fuel Cell Technology & Applications Conference report, it was estimated that startup/shutdown cycles contributed 44% to the degradation of PEMFC during practical operation.[2]

In 2005, United Technologies Corporation (UTC) proposed a reverse-current decay mechanism to explain the catalyst and catalyst support degradations during startups and shutdowns.[3] Many researchers developed current reversal models to describe the anode and cathode potential changes during the process.[4–7] Before startup, both cathode and anode are filled with air. When hydrogen (H_2) is introduced to the anode during startup, a H_2/air boundary is formed in the anode, which forces the cathode to reach a high half-cell potential of typically above 1.4 V. This high cathode potential causes severe carbon corrosion and results in considerable changes to the electrode morphology, e.g., electrode thinning, electrode collapse, platinum (Pt) agglomeration and dissolution, etc.[8] As a consequence, the cell performance suffered an irreversible deterioration.

Startup and shutdown in PEMFCs have been investigated under various operating conditions, such as different humidity levels, cell temperatures, and hydrogen flow rates.[9–11] Segmented cell technology was also applied to investigate the local current density distribution and to provide information for the cell degradation at different zones during SU/SD operations.[12] It was found that the carbon corrosion rates showed a linear increase with increasing reactant gas humidity. Furthermore, the corrosion phenomena were significant when the cell temperature was increased above 70 °C. Brightman et al. studied the effect of the anode H_2 flow rates on the carbon corrosion during SU/SD.[11] It was seen that during startups, as H_2 flow rate increased, less carbon corrosion was observed due to the reduced H_2/air front residence time. The magnitude and duration of the potential transient were decreased as well. Babu et al. evaluated the effect of platinum loading on both cathode and anode on the degradation of the electrode in SU/SD cycles.[13] They found that the electrode with higher platinum loading in the cathode while reducing the anode platinum loading proved to have reduced degradation during SU/SD cycling. Lower platinum loading in the anode reduced the current reversal by limiting oxygen reduction reaction (ORR) and hence reduced the carbon corrosion. The carbon corrosion at the cathode outlet was more severe than the inlet region. These studies enhanced fundamental understanding of carbon corrosion during SU/SD and thus guided the development of mitigation strategies.

The application of strategies to mitigate the degradation of the electrode is usually required for PEMFC systems, especially for transportation systems undergoing thousands of startup and shutdown events during their lifetimes. The solutions mainly focus on material innovations for the catalyst layer and system control strategies development. There has been extensive research to investigate more stable catalyst support materials. For example, Yamashita et al. reported that Pt catalysts supported on a graphitized carbon black presented an improved durability in SU/SD operations.[14,15] Uchida et al. proposed the use of ceramic nanoparticles in the anode because of the significant reduction of the reverse current due to the high resistivity of the ceramic in the air.[16] While the research on novel materials remains active, system control strategies may be more practical to alleviate or even avoid performance decay during SU/SD operations and prolong the fuel cell lifetime, especially from an automotive OEM's perspective. Yu et al. reviewed the causes and consequences of the performance degradation in SU/SD and reported the most common strategies involved: 1) minimizing the residence time of the H_2/air front at the anode, 2) completely preventing the H_2/air front at the anode, and 3) controlling the cathode potential.[17] H_2 purge and O_2 consumption on the cathode using a load were found to be the most effective

*Electrochemical Society Member.
†Deceased.
zE-mail: jchen186@ford.com

strategies.[18–21] Most studies focused on the development of a specific strategy with an end-of-life evaluation to confirm effectiveness, and fundamental knowledge of the degradation process and mechanism with and without the mitigation strategy still lacks.

This paper investigates three scenarios of SU/SD: startup and shutdown with air supply and soak to both anode and cathode (air-SU/SD), hydrogen protected startup and shutdown (H_2-SU/SD), and hydrogen protected startup and shutdown with a load (H_2-SU/SD with a load). The performance loss, electrochemical surface area (ECSA) degradation, and ohmic resistance change during SU/SD cycling were characterized. The temperature effect on air-SU/SD was studied in a wide range from 20 °C to 70 °C. Comprehensive failure analysis was performed to aid the understanding of degradation mechanism. The mechanism of H_2 protected SU/SD was discussed in comparison with unprotected SU/SD. Besides quantifying the effectiveness of H_2 protected SU/SD, this paper aims to provide comprehensive data along with detailed failure analyses to reduce the knowledge gap on SU/SD degradation mechanism with and without mitigation strategy and to facilitate future enhancement of system strategies on SU/SD durability.

Experimental

SU/SD protocols.—Three fuel cell vehicle SU/SD scenarios were investigated in this study with protocols schematically shown in Fig. 1. Due to the limited resource and the objective of fundamental study, SU/SD protocols were designed to represent the vehicle key-off/key-on cycles in an accelerated stress test (AST) fashion on a fuel cell test stand. An SU/SD protocol includes four steps to be one cycle: fuel cell operation, shutdown, soak, and startup. Figure 1a shows an air-SU/SD cycle, which simulates an unprotected shutdown of the vehicle, with air diffused into anode. After FC operation for 60 s reaching a steady state, shutdown started with closing gas supplies and disconnecting the load. As a result, voltage increased to open circuit voltage (OCV), which lasted 10 s. Then, air was introduced to the anode and cell voltage dropped. The cell was soaked under air/air in anode/cathode for 60 s. In the subsequent startup, air supply to the anode was stopped and hydrogen was supplied to the anode, which led to the traditional carbon corrosion scenario with air-hydrogen front in the anode.[3] This startup condition lasted 10 s, and then the cell was back to fuel cell operation at 0.4 A cm^{-2} for 60 s, which became the beginning of the next cycle.

In order to enhance the durability from unprotected SU/SD or air-SU/SD, hydrogen protected SU/SD (H_2-SU/SD) has been designed. Figure 1b illustrates such a protocol. The fuel cell operation remained the same and the shutdown started with dropping the flows and the load to zero which lasted 10 s. Then, H_2 supply on the anode was reopened as the beginning of H_2 purge and air supply on the cathode remained closed. H_2 permeated from the anode to the cathode through the membrane, creating a H_2 soak with the remaining O_2 in the cathode slowly consumed by H_2, while the cell voltage gradually dropped towards zero. H_2 purge remained during the whole shutdown period of 300 s, after which the startup initiated. The air supply to the cathode was reopened for 10 s, followed by the fuel cell operation transitioning to the next H_2-SU/SD cycle.

Figure 1c illustrates a H_2-SU/SD with a load as a further protection. After 10 s of shutdown conditions, a small load of 3 A or 0.075 A cm^{-2} was applied for 3 s to consume cathode O_2 quickly, during which both anode and cathode supplies were shut off and the cell voltage dropped towards zero. Then, the cell was soaked with H_2 purging to anode for 60 s, followed by startup and fuel cell operation to begin the next cycle.

For three SU/SD protocols in this study, the fuel cell operation and the startup were under the same conditions. In the fuel cell operation, a 0.4 A cm^{-2} load was added with a H_2 flow rate of 1 standard liter per minute (SLPM) on the anode and an air flow rate of 2 SLPM on the cathode. In the startup, 1 SLPM H_2 was supplied to the anode and 2 SLPM air flowed through the cathode. The operating conditions for shutdown and soak were different for three SU/SD protocols, as can be found in Table I. The temperature remained unchanged and back pressure was not applied throughout a test composed of 0.4 A cm^{-2} operation, shutdown, soak and startup. In addition, a relative humidity (RH) of 100% on both anode and cathode inlets was maintained, whenever there was gas supply.

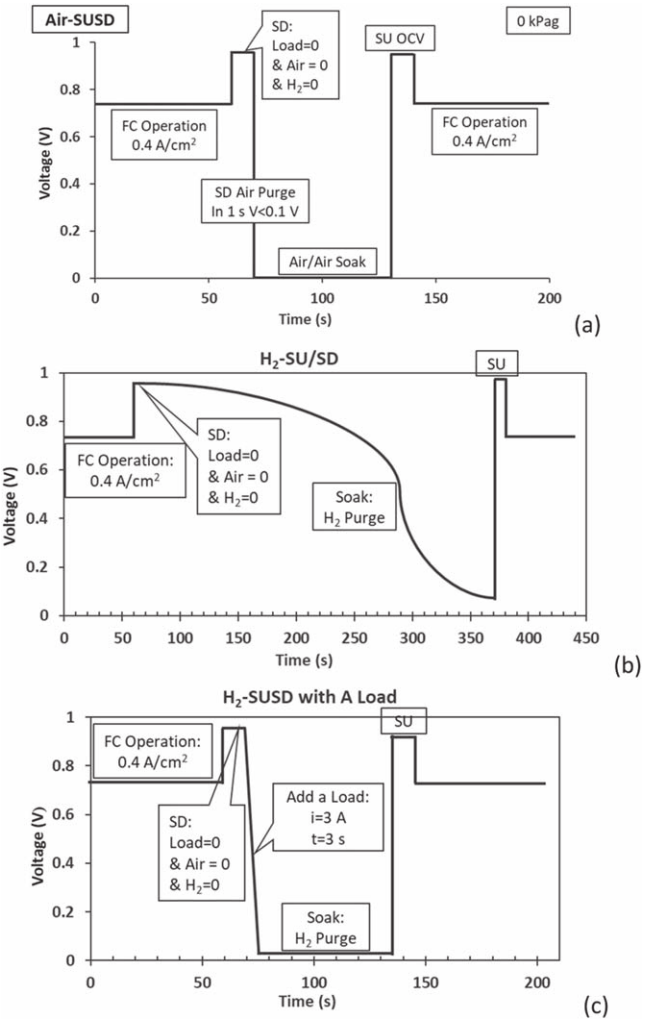

Figure 1. Schematics of three startup and shutdown protocols: (a) air-SU/SD; (b) H_2-SU/SD; and (c) H_2-SU/SD with a load. An SU/SD cycle consists of a fuel cell operation at 0.4 A cm^{-2}, a shutdown, a soak with either air or H_2, and a startup.

Materials and procedures.—A commercial PtCo catalyst coated membrane (CCM) with high-surface-area carbon support was used in this study. The catalyst loadings were 0.25 mg_{Pt} cm^{-2} for the cathode and 0.05 mg_{Pt} cm^{-2} for the anode. A 15 μm reinforced PFSA membrane was used as the polymer electrolyte membrane. The CCM was sandwiched between two gas diffusion layers (GDLs, SGL 29BC) to prepare the membrane electrode assembly (MEA) in-house, which was then assembled into a differential core attribute testing (CAT) cell for the SU/SD testing. CAT cell has an active area of 40 cm^2 and straight flow channels with 112.5 mm length, 0.25 mm width, and 0.4 mm depth on the cathode plate and 0.24 mm depth on the anode plate.

The test procedures for three SU/SD protocols are outlined in Fig. 2. The fresh MEA was firstly conditioned under 1.2 A cm^{-2} under 60 °C and 100% RH for 12 h. The diagnostics for beginning of life (BOL), inter-cycling, and end of life (EOL) included electrochemical surface area (ECSA), polarization at 1.2 A cm^{-2} (mass transport region) and 0.02 A cm^{-2} (kinetic region), and high frequency resistance (HFR).

Table I. The operating conditions for shutdown and soak processes during SU/SD cycling.

Parameter	Unit	Air-SU/SD	H_2-SU/SD	H_2-SU/SD-3A
Anode Concentration	mol%	O_2: 21	H_2: 100	H_2: 100
Anode Flow Rate	SLPM	2	8	4
Anode RH	%	100	100	100
Cathode Concentration	mol%	O_2: 21	N/A	N/A
Cathode Flow Rate	SLPM	2	0	0
Cathode RH	%	100	N/A	N/A
Coolant Flow Rate	SLPM	1	1	1
Load	A cm^{-2}	0	0	0.075
Temperature	°C	20/35/55/70	35	35
Pressure	KPag	0	0	0

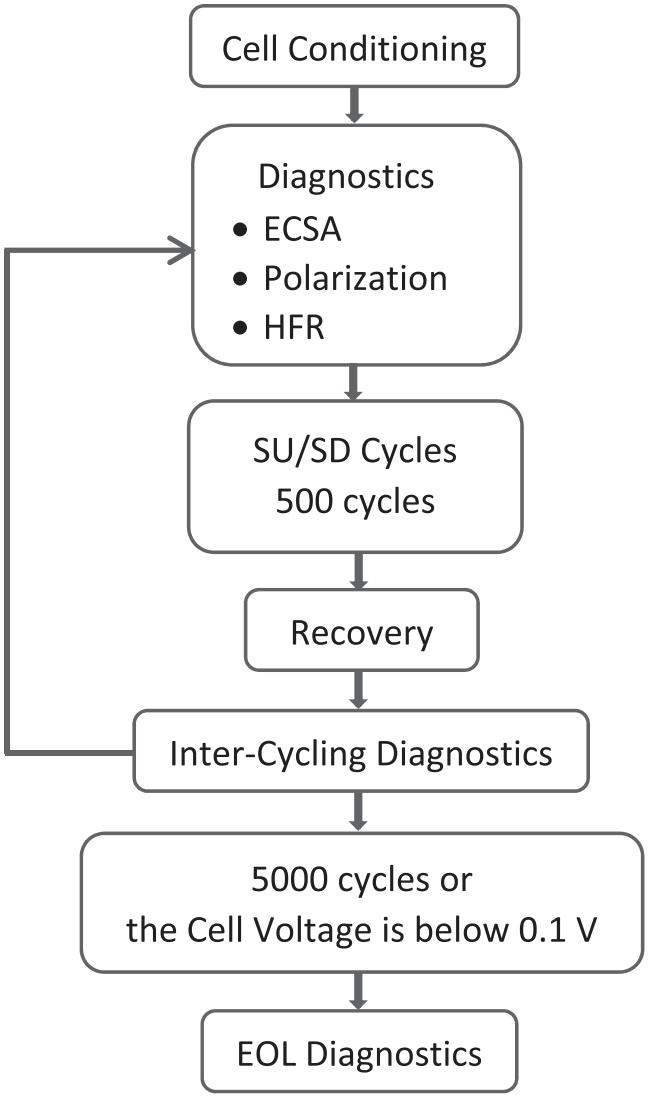

Figure 2. The SU/SD test procedures.

ECSA was evaluated by cyclic voltammetry (CV) under 80 °C and 100% RH with 4 SLPM H_2 on the anode and 8 SLPM N_2 on the cathode with a potentiostat (Zahner IM6). The anode was used as both reference electrode and counter electrode for the CV. The cathode potential was swept at 20 mV s^{-1} from 0.05 V to 0.6 V. The value of ECSA was determined from the average of the hydrogen adsorption charge and the hydrogen desorption charge with 0.21 mC cm^{-2}_{Pt} to desorb a monolayer of hydrogen on Pt. The charging current (double layer capacitance times scan rate) and hydrogen crossover were subtracted by integrating the hydrogen desorption peaks only at currents above the current from the capacitive region. This means that the integration limits were therefore where the current exceeded the capacitive region (at lower voltage on the forward sweep) and where the current decreased back down to the capacitive region current (at higher voltage on the forward sweep). This proceeded similarly for integrating the adsorption peaks on the reverse sweep where the higher voltage integration limit is where the current becomes more negative than the capacitive region current on the reverse sweep. For the lower voltage integration limit on the adsorption peaks, because of the adsorption peak convolution with hydrogen evolution peaks, a macro was used to determine when the slope of the current would increase again at progressively lower voltage, and at that voltage the integration limit was drawn so as to eliminate the charge associated with hydrogen evolution. Polarization was performed at 80 °C and 100% RH under 1 SLPM H_2 and 2 SLPM air with 150 Kpa gauge on both sides. A constant load of 1.2 A cm^{-2} was applied for 30 min when HFR was measured under this load. The average value of the recorded cell voltages in the last minute of current hold was used to plot the polarization. HFR was measured with a frequency sweep range from 100 mHz to 100 kHz under the amplitude of 10 mV with the potentiostat. The HFR (Ω) was obtained when the imaginary part of impedance was minimized. The value of HFR in mΩ·cm^2 was calculated by multiplying the impedance value by active area and dividing by 1000.

Every 500 SU/SD cycles, diagnostics were performed to evaluate the degradation. If the cell voltage at 1.2 A cm^{-2} dropped below 0.1 V, the cell was considered to have reached lifetime. Otherwise, cycling continued until 5000 cycles were completed. Some tests concluded before cycling to 5000 cycles due to inability of the MEA to sustain performance during cycling or due to other control issues. Before diagnostics, an MEA recovery protocol from US DRIVE Fuel Cell Tech Team[22] was applied to recover the reversible losses through Pt reduction and to ensure a consistent catalyst condition.

SEM, TEM and STEM measurements.—Scanning electron microscopy (SEM) was performed at the University of Connecticut with the following steps. After embedding a 2 cm × 1 cm section of the MEA in EpoThin epoxy resin (BUEHLER, USA), the section was grinded in an automated polishing machine (Struers LaboPro-5, Denmark) using 60-, 240-, 600-, and 1200-mesh silicon carbide grinding papers followed by polishing the block by 0.1 μm alumina polishing paste (BUEHLER, USA). The mirror-like surface of the sample was then gold coated for a few nanometers (Denton Vacuum LLC, USA). The cross-sectional SEM imaging was completed by a Teneo LV Scanning Electron Microscope (SEM, Thermo Fisher Scientific, USA) using the circumferential backscattered (CBS) detector at electron accelerating voltage and beam current of 15 kV and 0.8 nA, respectively, at two different magnifications. The cathode, membrane, and anode thicknesses were measured by the aid of open source Fiji ImageJ software using at least 7 images at 5000× magnification. For each image, at least ten different sites of each

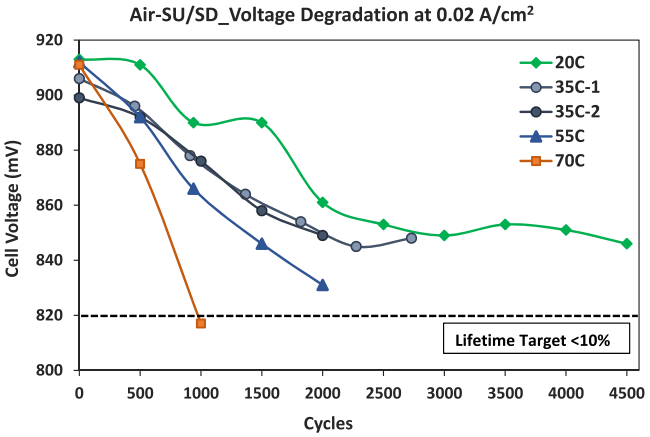

Figure 3. The voltage degradation at 0.02 A cm^{-2} during air-SU/SD at different temperatures. A repetition was conducted for 35 °C.

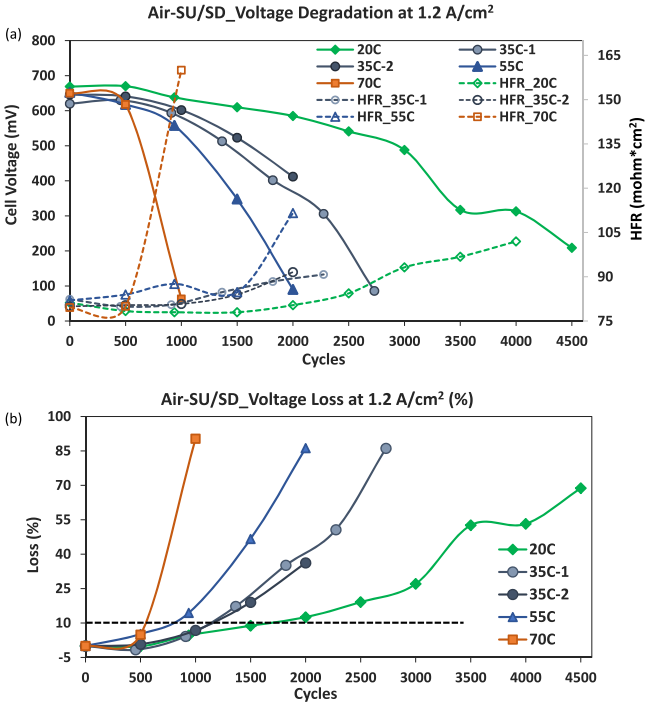

Figure 4. The voltage degradation at 1.2 A cm^{-2} during air-SU/SD at different temperatures. (a) Cell voltage values along with HFR in the cycling. (b) Voltage loss percentage drop during cycling.

layer were measured. Finally, the mean thickness value along with the corresponding entire population standard deviation was reported.

The catalyst layer morphology and the degradation of Pt nanoparticles were evaluated by transmission electron microscopy (TEM) and scanning transmission electron microscopy with energy

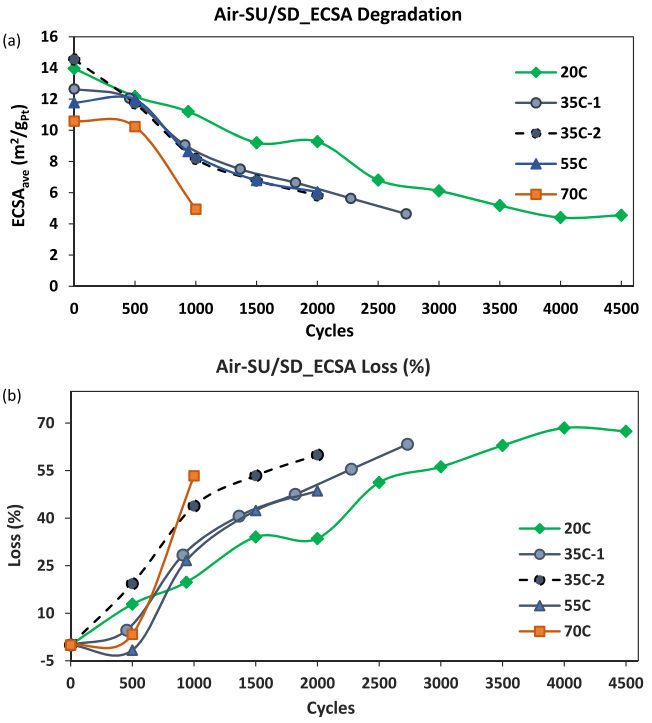

Figure 5. The ECSA degradation in air-SU/SD at different temperatures. (a) Averaged ECSA values in the cycling. (b) ECSA loss percentage drop in cycling.

dispersive spectroscopy (STEM-EDS). For TEM sample preparation, the GDLs were peeled off from the CCM with the aid of a tweezer, and then a 1 cm × 0.5 cm section of the CCM was cut with scissors. A small piece of the catalyst coated membrane was embedded in a 1:1 mixture of trimethylolpropane triglycidyl ether resin (Sigma-Aldrich, USA) and 4,4′-Methylenebis (2-methylcyclohexylamine, Sigma-Aldrich, USA) hardener and polymerized overnight in a 60 °C oven to prepare the block for the microtome. Thin sections (approximately 100 nm) were cut by Leica UCT ultramicrotome setup (Germany) equipped with an Ultra 45°DiATOME knife, USA. The sections were situated onto multiple 200 mesh Cu/Pd grids. A Talos F200X scanning transmission electron microscope (STEM, Thermo Fisher Scientific, USA) equipped with Super-X four silicon drift detectors of energy dispersive X-ray spectrometry (Super-X SDD EDXS, Bruker, USA) at solid angle of 0.9 steradian with electron accelerating voltage of 200 kV was utilized for imaging and elemental mapping of the sample. The TEM images at 190kx magnification and 1024 pixel × 1024 pixel resolution were acquired from at least 4 different random regions by the bright field detector (BF-TEM). The total number of 200 platinum particles were measured by Fiji ImageJ to extract the particle-size distribution (PSD). The EDS mapping was done on a 768 pixel × 768 pixel region, at 5kx and 79kx magnifications, with a 1000 μs dwell time for 1 cycle and electron dose of 2.34 × 104 e^{-}/nm^{2}. Further elemental analysis and raw data extraction were carried out by the ESPIRIT 1.9 (Bruker, USA) analytical software. While more details

Table II. Summary of voltage loss and ECSA loss for air-SU/SD at different temperatures.

Attribute	Unit	Air-SU/SD_20C	Air-SU/SD_35C	Air-SU/SD_55C	Air-SU/SD_70C
ECSAave_BOL	m^2/gPt	13.96	12.65	11.77	10.60
V1.2 A cm^{-2}_BOL	mV	669	646	652	650
V loss at 1.2 A cm^{-2} after 2000 cycles	mV	84	266	562	>587
V loss at 0.02 A cm^{-2} after 2000 cycles	mV	52	60	81	>94
ECSAave loss after 2000 cycles	m^2/gPt	4.69	6	6	>6
Life time	Cycle	5000	2700	2000	1000

Table III. The catalyst layer thickness changes in air-SU/SD at different temperatures.

	BOL	Air-SU/SD_35C	Air-SU/SD_70C
SEM	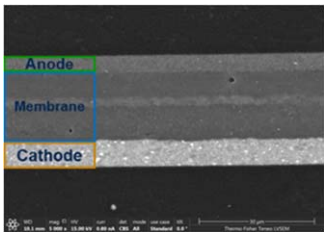	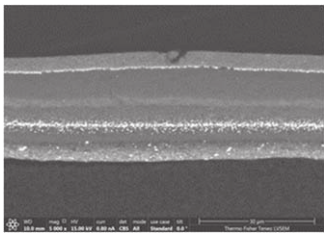	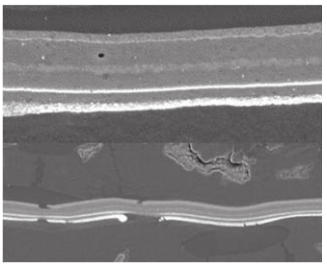
Cathode (μm)	7.3 ± 0.3	5.2 ± 0.2 (−29%)	3.4 ± 1.1 (−53%)
Membrane (μm)	16.6 ± 0.4	17.7 ± 0.3	16.6 ± 0.6
Anode (μm)	3.8 ± 0.3	3.9 ± 0.3	3.6 ± 0.8

of the sample characterization method can be found in another publication,[23] the numerical quantification of the sample was conducted by an in-house developed proprietary technique in order to see the changes in the sample after cycling.

Results and Discussion

Performance degradation of air-SU/SD at different temperatures.—Air-SU/SD was studied in a wide range of temperatures. Table II summarizes the BOL performance and the performance losses after 2000 cycles for different cells with different temperatures. The BOL ECSA varied within a standard deviation of 1.4 m^2/gPt and the cell voltage at 1.2 A cm^{-2} varied within a standard deviation of 10 mV, which confirmed that these cells had consistent BOL performances. Figures 3 and 4 show the performance degradations at 0.02 and 1.2 A cm^{-2}, respectively, from air-SU/SD cycling; and Fig. 5 illustrates the ECSA losses. In the entire range of 20 °C–70 °C, temperature has a significant impact upon performance losses associated with air-SU/SD. The voltage losses increased dramatically with increasing temperatures in comparing all performances after 2000 cycles. At 20 °C and 1.2 A cm^{-2}, the loss was 84 mV. When temperature increased to 35 °C, the voltage loss increased to 266 mV. At 55 °C, the voltage loss increased to 562 mV. At 70 °C, the cell only survived 1000 cycles as it was unable to reach 100 mV. In addition, at the final diagnostic the HFR increased dramatically to 160 mohm × cm^2 and ECSA lost about 55% of its initial value. From the SEM images for 70 °C in Table III, a Pt band is visible in the membrane close to the cathode, along with a substantially reduced cathode thickness and catalyst layer rupture at some spots. Hence, the HFR increase could be related to the reduced protonic conductivity in the membrane due to the Pt band and the reduced electronic conductivity due to the poor contact of catalyst layer with membrane and GDL. ECSA losses exhibited a similar temperature impact. Shown in Fig. 5b, ECSA losses at 35 °C and 55 °C fell between those at 20 °C and 70 °C.

As shown in Table II, when the temperature reduced to 20 °C, the cell could complete 5000 cycles of air-SU/SD cycling before the cell voltage dropped below 100 mV. If 10% power loss is considered the lifetime for a cell, the cell was able to survive about 1700 air-SUSD cycles at 20 °C shown in Fig. 4b. Temperature seems to be a very effective system parameter to prolong the air-SU/SD lifetime. An unprotected air SU/SD could exhibit three-folded difference in lifetime from 20 °C to 70 °C, which could be utilized in projecting lifetime and developing system strategies.

Catalyst degradation in air-SU/SD at different temperatures.—In order to understand the cause of performance loss in air-SU/SD cycling, SEM and TEM of BOL and EOL samples were performed. Table III shows SEM images and catalyst layer thickness changes in air-SU/SD at 35 °C and 70 °C. A Pt band formed in the membrane and the thickness of cathode catalyst layer decreased substantially. At 35 °C, about 29% of the cathode thickness was lost compared with a BOL sample. When temperature increased to 70 °C, the cathode lost more than 50% thickness, along with some discontinuity of the cathode catalyst layer due to severe degradation. The Pt band appeared wider and brighter, indicating greater amount of Pt reduction. The membrane and anode thickness changes were minor from air-SU/SD cycling at all temperatures.

STEM-EDS maps and characteristics of the cathode catalyst layer are summarized in Table IV. After air-SU/SD cycling, Pt and

Table IV. The catalyst degradation in air-SU/SD at different temperatures.

	BOL	Air-SU/SD_35C	Air-SU/SD_70C
TEM (Cathode)	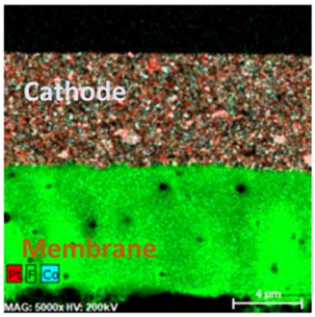	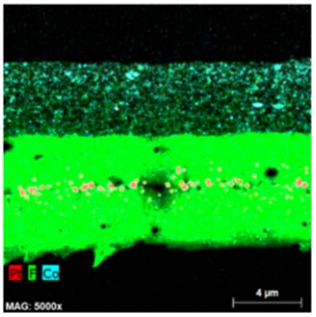	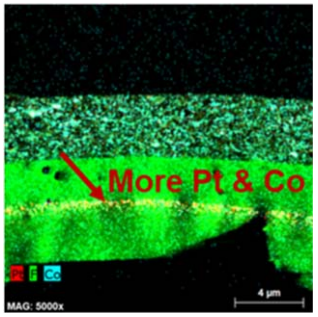
Ave Particle Size (nm)	5.40 ± 2.71	7.25 ± 3.84	9.03 ± 6.57
Pt Loading (mgPt cm^{-2})	0.20	0.09	0.09
Pt/Co Atomic Ratio	3.29	3.68	3.6

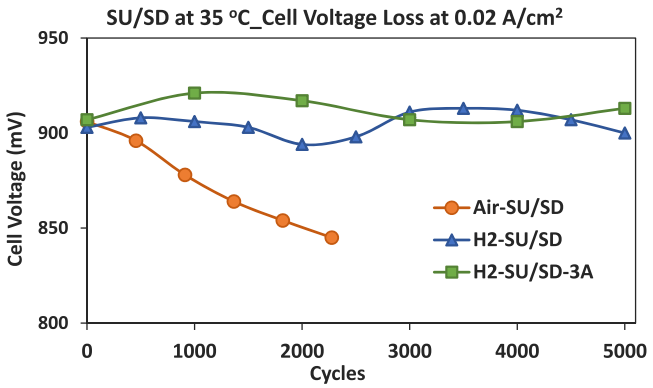

Figure 6. The cell voltage degradation at 0.02 A cm^{-2} during SU/SD at 35 °C.

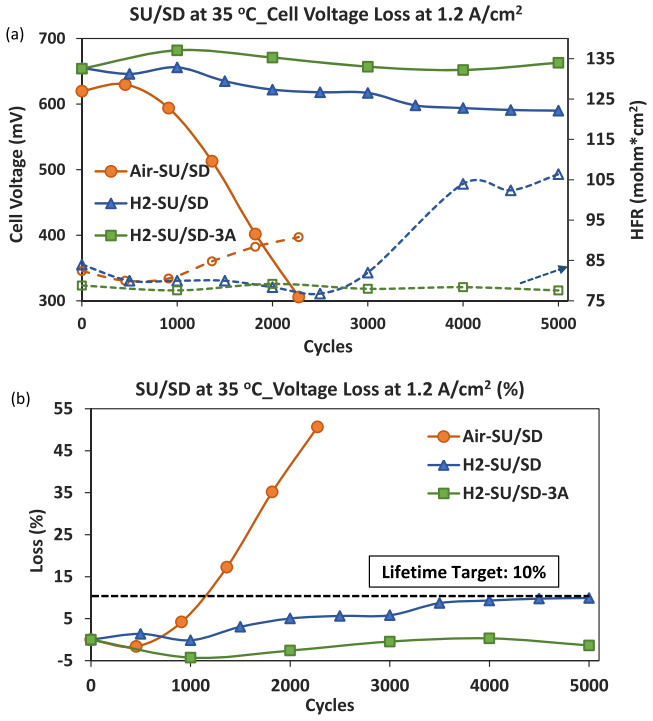

Figure 7. The voltage degradation at 1.2 A cm^{-2} during SU/SD at 35 °C. (a) Cell voltage along with HFR in the cycling. (b) Voltage loss percentage during cycling.

Co were detected in the membrane. Pt loading in the catalyst layer decreased by more than 50% and the Pt/Co ratio increased, as quantified from the EDS maps. The increase of Pt/Co as compared to BOL probably indicated a faster rate of Co leaching along with the Pt dissolution, due to the thermodynamic instability of Co in fuel cell conditions. At higher temperature of 70 °C, the existence of Pt and Co in the membrane was more pronounced. A Pt band was visible in the membrane. Leached Co from cathode alloy catalyst was distributed throughout the membrane. Furthermore, Pt particle size increased substantially from air-SU/SD cycling, with 70 °C accelerating Pt particle growth. Given that at 70 °C the cell failed at 1000 cycles whereas at 35 °C it failed over 2000 cycles, the temperature effect on Pt dissolution and coalescence was quite strong. With combined evidences from SEM, STEM-EDS, and particle size, it could be confirmed that Pt dissolution occurred through Ostwald ripening, migration and coalescence in air-SU/SD cycling along with the carbon corrosion.

It is well-known that during air/air SU a hydrogen/air front is formed in the anode, and severe carbon corrosion could happen in

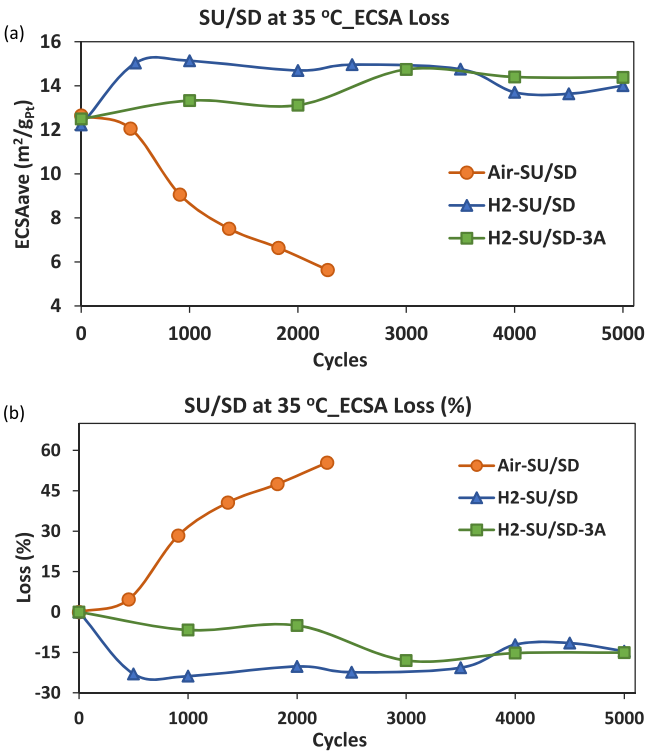

Figure 8. The ECSA degradation in SU/SD at 35 °C. (a) Averaged ECSA values in the cycling. (b) ECSA loss percentage in cycling.

the cathode. The carbon loss could lead to reduced catalyst layer thickness. Table V lists SEM images and thickness losses at different location of the cell after air-SU/SD cycling at 70 °C. The loss of cathode catalyst layer thickness at the middle and outlet of the cell was consistent with the existing knowledge, as the opposite anode of those regions had experienced longer exposure to H_2/air front.

Performance degradation of three SU/SD protocols at 35 °C.— In addition to air-SU/SD protocol, hydrogen protected SU/SD (H_2-SU/SD) was also investigated. To quantify the effect of quickly depleting oxygen during shutdown, another protocol with a small load of 3 A (H_2-SU/SD-3A) was tested. In this subsection, these SU/SD protocols are compared at 35 °C. Figures 6 and 7 present the cell voltage degradation at 0.02 and 1.2 A cm^{-2}, respectively. Hydrogen protected SU/SD protocols (H_2-SU/SD and H_2-SU/SD-3A) effectively preserved the cell performance compared with air-SU/SD protocol. At 35 °C, the cell failed with ~2700 cycles in air-SU/SD cycling. As summarized in Table VI, when the cell failed from air-SU/SD, at 0.02 A cm^{-2} the cell voltage lost about 60 mV and at 1.2 A cm^{-2} it lost more than 250 mV, which was more than 35% drop of BOL performance. In hydrogen protected SU/SD, after 5000 cycles, the cell performance was maintained in the kinetic region and the performance loss was less than 10% in the mass transport region. H_2-SU/SD-3A cycling somehow improved the cell performance slightly probably due to the enhanced accessibility of inner catalytic active area with minor carbon loss. Clearly, both H_2 protected protocols were able to minimize the SU/SD degradation and prolong the unprotected SU/SD lifetime by a factor of approximately 4. Figure 8 plots ECSA changes in these three SU/SD protocols. ECSA exhibited similar degradation behaviors as observed for performance. After 2000 cycles of air-SU/SD, ECSA decreased more than 60%. On the contrary, ECSA was preserved in hydrogen protected SU/SD protocols.

Catalyst degradation of three SU/SD protocols at 35 °C.—The failure analysis of the catalyst layer from these SU/SD protocols was performed with SEM and TEM. Table VII summarizes SEM images

Table V. The catalyst layer thickness changes in different regions of the cell during air-SU/SD at 70 °C.

	BOL	Inlet	Middle	Outlet
SEM	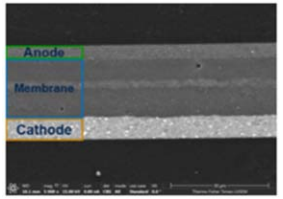	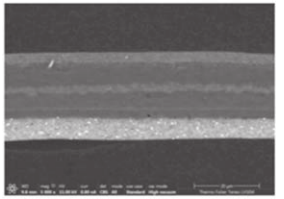	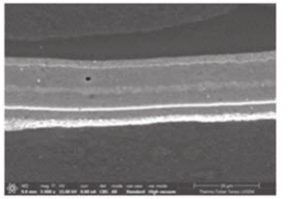	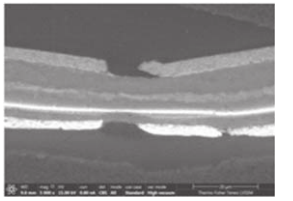
Cathode (μm)	7.3 ± 0.3	6.3 ± 0.7 (−14%)	3.4 ± 1.1 (−53%)	3.5 ± 1.1 (−52%)
Membrane (μm)	16.6 ± 0.4	17.4 ± 0.9	16.6 ± 0.6	17.4 ± 0.4
Anode (μm)	3.8 ± 0.3	3.8 ± 0.3	3.6 ± 0.8	4.1 ± 0.2

Table VI. Summary of voltage losses for three SU/SD processes at 35 °C.

Attribute	Unite	Air-SU/SD_35C	H_2-SU/SD_35C	H_2-SU/SD-3A_35C
V loss at 1.2 A cm^{-2} after ~2000 cycles	mV	266	33	−17
V loss at 0.02 A cm^{-2} after ~2000 cycles	mV	60	9	−10
V loss at 1.2 A cm^{-2} after 5000 cycles	mV	—	65	−9
V loss at 0.02 A cm^{-2} after 5000 cycles	mV	—	3	−6
Lifetime	Cycle	~2700	>5000	>5000

and catalyst layer thicknesses of the BOL and EOL MEAs. At 35 °C, after 2000 cycles of air-SU/SD, cathode catalyst layer lost about 29% thickness compared with BOL catalyst layer. In H_2-SU/SD and H_2-SU/SD-3A, after 5000 cycles, the thickness of the cathode catalyst layer decreased 8%–9%, confirming that carbon corrosion had been mitigated in hydrogen protected SU/SD protocols. From air-SU/SD cycling, Pt depleted heavily from the cathode and formed a Pt-rich band in the membrane. Pt-depleted region in the cathode is shown as a darker region indicated by the arrow in Table VII. These effects were not observed for H_2 protected protocols. TEM images and catalyst layer characteristics are shown in Table VIII. From air-SU/SD, it can be observed that Pt and Co migrate into the membrane (confirmed by STEM-EDS mapping). The cathode catalyst layers from H_2-SU/SD and H_2-SU/SD-3A did not seem to have major differences from the BOL catalyst layer. Co leaching seemed to have occurred from all SU/SD protocols due to its thermodynamic instability in a fuel cell. The amount of Co loss was thus dependent on the total test time. Therefore, the end-of-life samples from H_2 protected protocols, which had gone through longer test time and less Pt loss compared with air-SU/SD sample, exhibited greater Pt/Co ratios. Furthermore, the Co loss from the H_2 protected protocols could explain the greater Pt/Co ratios as compared to BOL, despite the minor change of Pt under H_2 protection. The averaged particle sizes from the three protocols seem to indicate that both H_2 protected protocols still led to Pt dissolution and coalescence to some extent, although the high standard deviations and the local-area statistics should be noted. In addition, H_2 protected protocols had gone through 5000 cycles as compared to 2000 cycles for unprotected air-SU/SD, which may have contributed to the similar Pt particle sizes for air-SU/SD and H_2-SU/SD-3A.

Mechanism of catalyst degradations in three SU/SD protocols.—In this subsection, reaction mechanisms are discussed for different SU/SD protocols. Figure 9 compares reactions during air-SU/SD vs H_2-SU/SD. In an unprotected air/air startup (Fig. 9a), as hydrogen is supplied to the anode, a H_2/air front develops and moves through the channel. Since this is a traditional SU/SD scenario well known in literature, further discussion is not provided besides a note that Pt dissolution could also occur on the cathode along with carbon corrosion.

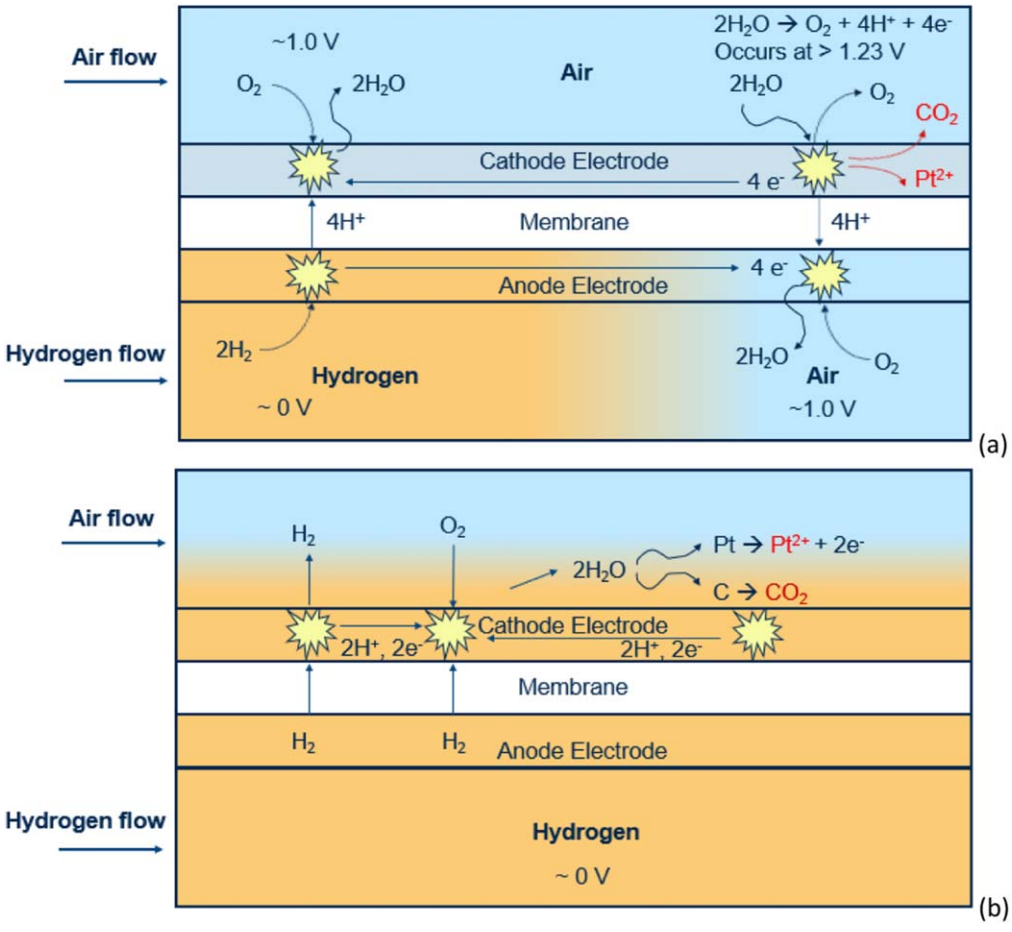

Figure 9. The diagram of electrode reactions during startup processes. (a) Air/air SU. (b) H_2/air SU.

Table VII. The catalyst layer thickness changes during SU/SD processes at 35 °C.

	BOL	Air-SU/SD	H_2-SU/SD	H_2-SU/SD-3A
SEM	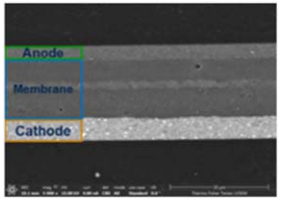	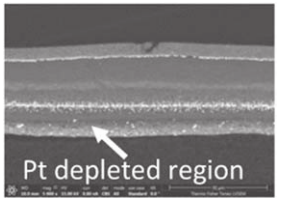	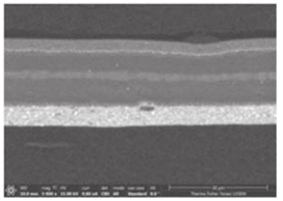	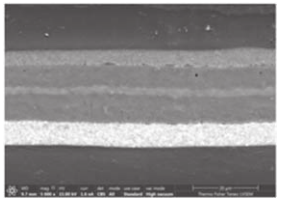
Cathode (μm)	7.3 ± 0.3	5.2 ± 0.2 (−29%)	6.7 ± 0.2 (−8%)	6.6 ± 0.6 (−9%)
Membrane (μm)	16.6 ± 0.4	17.7 ± 0.3	17.4 ± 0.4	17.2 ± 0.6
Anode (μm)	3.8 ± 0.3	3.9 ± 0.3	4.1 ± 0.2	4.3 ± 0.8

Table VIII. The catalyst degradation during SU/SD processes at 35 °C.

	BOL	Air-SU/SD	H_2-SU/SD	H_2-SU/SD-3A
TEM (Cathode)	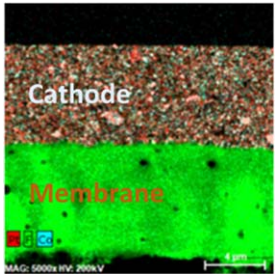	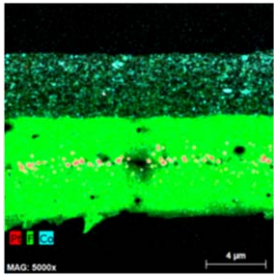	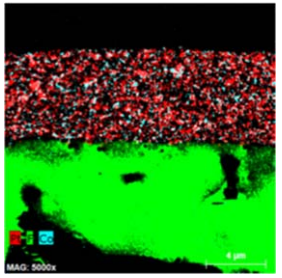	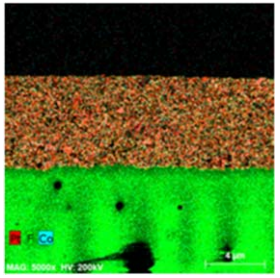
Pt Distribution	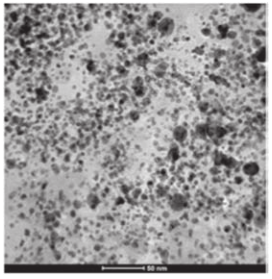	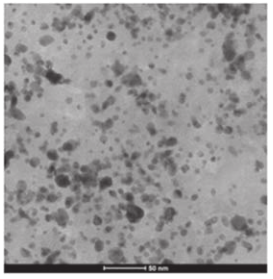	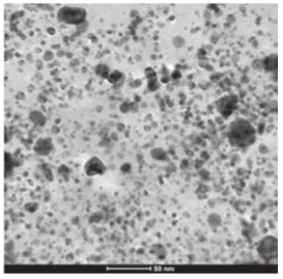	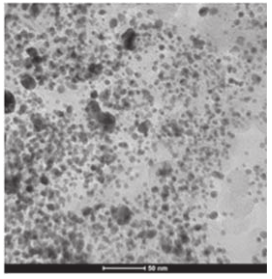
Pt Particle Size Distribution	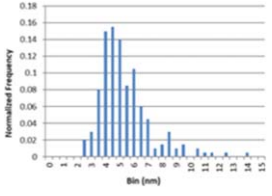	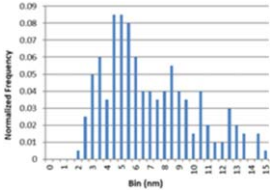	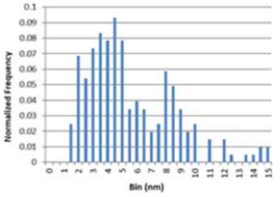	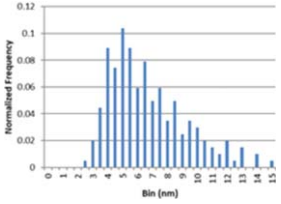
Ave Particle Size (nm)	5.40 ± 2.71	7.25 ± 3.84	6.03 ± 4.44	7.28 ± 4.36
Pt Loading (mgPt cm^{-2})	0.20	0.09	0.19	0.16
Pt/Co	3.29	3.68	4.87	4.51

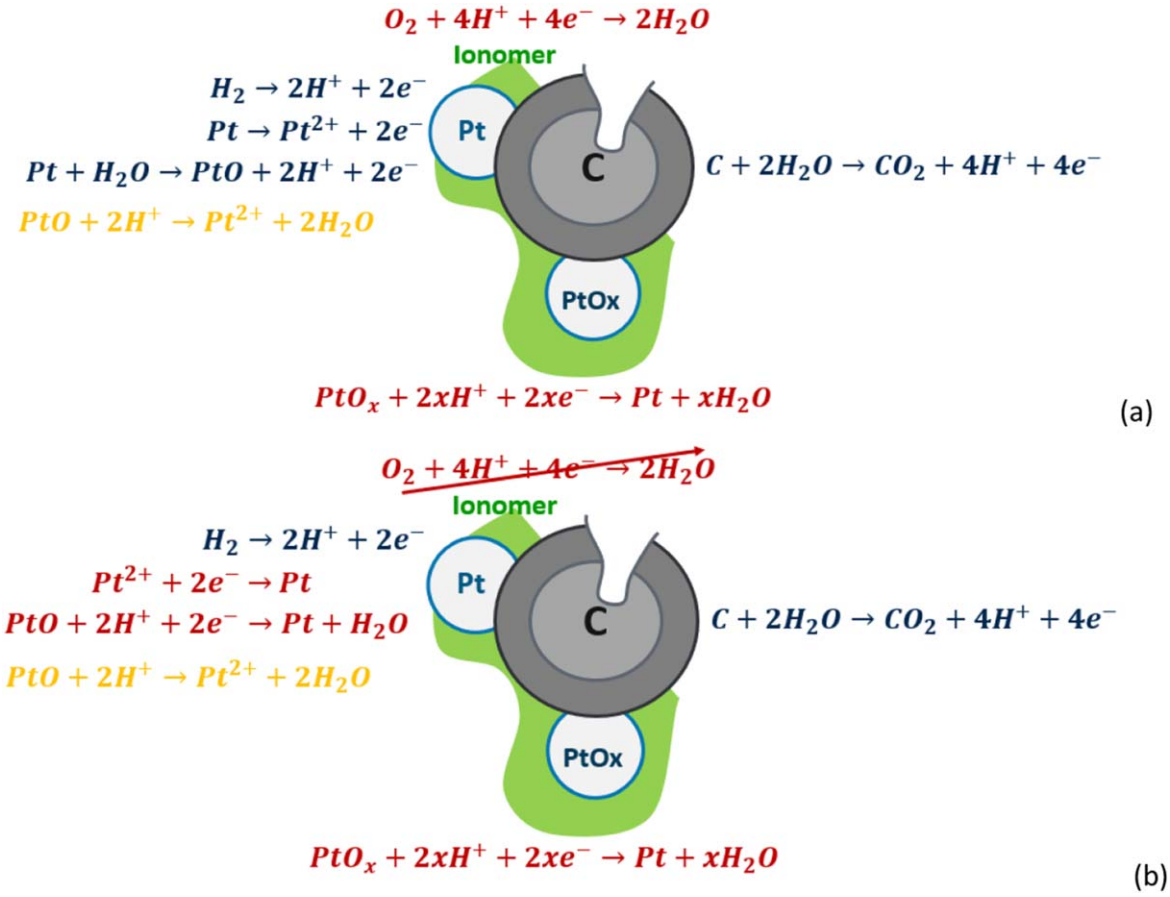

Figure 10. The reaction mechanisms during a H_2 purge shutdown (a) without a load; (b) with a load. Reactions in blue are oxidation reaction supplying protons and electrons, which are consumed by reduction reactions in red. The chemical reactions are in yellow in contrast to electrochemical reactions. The illustration is a representative snapshot of the long H_2 soak and voltage drop process.

In a H_2 protected SU/SD, hydrogen is delivered to anode and then permeated to cathode before the startup. The current reversal mechanism in an unprotected startup is disabled since air is not available in the anode. During startup, normal HOR takes place in the anode and ORR occurs in the cathode as shown in Fig. 9b. The majority of protons needed for ORR is provided by HOR. However, the consumption of protons and electrons by ORR could still drive a carbon corrosion reaction locally at the Pt/C interface, such as a site without ionomer coverage and thus lacking proton transport, as long as water is available as another reactant. Nevertheless, carbon corrosion in this scenario proceeds slowly due to the facile process of HOR to electrochemically balance ORR, which is the fundemantal mechanism for H_2 protection. This explanation may be also applicable to a literature finding that carbon corrosion may occur due to unevenly distributed ionomer.[24]

In H_2-SU/SD, there was a slow depletion of cathode oxygen through the reaction with crossover hydrogen, which still led to certain amount of carbon corrosion. Thus, a load was added in shutdown to bleed down oxygen quickly. Figure 10 explains the reaction mechanisms during the shutdown processes of H_2-SU/SD vs H_2-SU/SD-3A. For H_2-SU/SD without a load, the cell voltage dropped slowly from open circuit voltage (OCV) to less than 0.1 V while hydrogen permeated from anode to cathode. The crossover H_2 was able to consume the cathode O_2 chemically and electrochemically. The electrochemical pathway refers to the proceeding of ORR at the cathode three-phase boundary, which was primarily paired with HOR, although carbon corrosion and Pt dissolution could have also occurred depending on the local potential, which was slowly decreasing from OCV at a H_2/air state. It should be noted shown in Fig. 10a is a snapshot of the long H_2 soak and voltage drop process; Pt oxidation reaction to PtO could be reversed with decreasing potential.[25]

When a load was applied before H_2 purge, which depleted remaining O_2 and reduced local potential quickly, the reaction to consume protons and electrons was PtOx and PtO reduction, as well as Pt cation reduction that consumes electrons, as illustrated in Fig. 10b. This may be a fast process as Pt oxide was consumed with fast-decreasing potential, during which HOR could provide the protons and electrons sufficiently, disabling the COR. On the other hand, the fast-decreasing potential substantially reduced the kinetics of COR while maintaining decent kinetics of HOR, given the difference of their thermodynamic equilibrium potentials. For these reasons, H_2-SU/SD with a load exhibited the best effect of mitigation.

Conclusions

This study investigated catalyst degradation behaviors in three SU/SD protocols: air-SU/SD, H_2-SU/SD and H_2-SU/SD with a load. Advantages with hydrogen protection and load drawn have been demonstrated with comprehensive test data and failure analysis. The air-SU/SD in a wide range of temperatures from 20 °C to 70 °C has been tested. As temperature increased, the voltage loss and ECSA loss increased dramatically. Failure analysis confirmed that the performance degradation in air-SU/SD cycling was from carbon corrosion and Pt dissolution. Both Pt and Co were observed in the membrane from air-SU/SD failed samples with visible Pt bands. Complete loss of cathode catalyst layer locally along with Pt band and much reduced catalyst layer thickness was observed for 70 °C, which is considered to cause the dramatically increased cell

resistance. H_2-SU/SD preserved the cell performance greatly after 5000 cycles, maintaining the performance loss within the 10% target and prolonging the lifetime of an unprotected air-SU/SD by a factor of approximately 4. The failure analysis confirmed mild degradations as compared to air-SU/SD based on electrode thickness, Pt/Co ratio, Pt loading and particle size. The H_2 purge and soak eliminated the high cathode potential from the current reversal in an air-SU/SD, therefore effectively suppressing carbon corrosion and Pt dissolution. However, as the remaining O_2 was consumed and voltage decreased slowly during the soak, certain amount of carbon corrosion and Pt dissolution may still exist. As the most effective strategy, H_2-SU/SD with a 3 A or 0.075 A cm^{-2} load consumed the remaining O_2 and dropped potential quickly, therefore showing negligible carbon corrosion, Pt dissolution and performance loss after 5000 cycles. Besides quantitatively confirming the benefits from H_2 protection and load drawn during shutdown, this study has provided comprehensive performance and failure analysis data together with thorough analysis of the mitigation mechanisms to aid the future enhancement of SU/SD strategies.

Acknowledgments

This work was entirely funded by Ford Motor Company. Technical support from Michael Potocki at Ford Motor Company is appreciated. TEM sample preparation from Marcia Reid at McMaster University, Canada is also appreciated. This work was primarily completed by Dr. Chunmei Wang before she suddenly passed away in September 2020 due to a health episode. This publication has been submitted in remembrance to an irreplaceable team member and a dedicated fuel cell researcher.

ORCID

Amir Peyman Soleymani https://orcid.org/0000-0002-6265-2296
Jixin Chen https://orcid.org/0000-0002-5020-8024

References

1. Y. C. Park, K. Kakinuma, M. Uchida, D. A. Tryk, T. Kamino, H. Uchida, and M. Watanabe, *Electrochim. Acta*, **91**, 195 (2013).
2. D. Low, L. M. Jackson, and S. J. Dunnett, *Proceedings of EFC2019* (2019).
3. C. A. Reiser, L. Bregoli, T. W. Patterson, J. S. Yi, J. D. Yang, M. L. Perry, and T. D. Jarvi, *Electrochem. Solid-State Lett.*, **8**, A273 (2005).
4. J. P. Meyers and R. M. Darling, *J. Electrochem. Soc.*, **153**, A1432 (2006).
5. H. Tang, Z. Qi, M. Ramani, and J. F. Elter, *J. Power Sources*, **158**, 1306 (2006).
6. J. E. Owejan, P. T. Yu, and R. Makharia, *ECS Trans.*, **11**, 1049 (2007).
7. J. Chen, J. Hu, and J. Waldecker, *J. Electrochem. Soc.*, **162**, F878 (2015).
8. T. Zhang, P. Wang, H. Chen, and P. Pei, *Appl. Energy*, **223**, 249 (2018).
9. J. H. Kim, E. Cho, J. H. Jang, H. Kim, T. Lim, I. Oh, J. J. Ko, and S. C. Oh, *J. Electrochem. Soc.*, **157**, B104 (2010).
10. Y. Y. Jo, E. Cho, J. H. Kim, T. Lim, I. Oh, S. Kim, H. Kim, and J. H. Jang, *J. Power Sources*, **196**, 9906 (2011).
11. E. Brightman and G. Hinds, *J. Power Sources*, **267**, 160 (2014).
12. R. Lin, X. Cui, J. Shan, L. Techer, F. Xiong, and Q. Zhang, *International J. Hydrogen Energy*, **40**, 14952 (2015).
13. S. K. Babu, D. Spernjak, J. Dillet, A. Lamibrac, G. Maranazna, S. Didierjean, O. Lottin, R. L. Borup, and R. Mukundan, *Appl. Energy*, **254**, 113659 (2019).
14. M. Hara, M. Lee, C. Liu, B. Chen, Y. Yamashita, M. Uchida, H. Uchida, and M. Watanabe, *Electrochim. Acta*, **70**, 171 (2012).
15. Y. Yamashita, S. Itami, J. Takano, M. Kodama, K. Kakinuma, M. Hara, M. Watanabe, and M. Uchida, *J. Electrochem. Soc.*, **163**, F644 (2016).
16. M. Uchida, K. Kakinuma, and A. Iiyama, *Nanostructured Materials for Next-Generation Energy Storage and Conversion* (Springer, Berlin) p. 53 (2018).
17. Y. Yu, H. Li, H. Wang, X. Yuan, G. Wang, and M. Pan, *J. Power Sources*, **205**, 10 (2012).
18. A. Oyarce, E. Zakrisson, M. Ivity, C. Lagergren, A. B. Ofstad, A. Boden, and G. Lindbergh, *J. Power Sources*, **254**, 232 (2014).
19. S. P. Kumaraguru, J. A. Rock, and B. Lakshmanan, *US Pat.*, 9,647,279 B2 (2017).
20. P. T. Yu and F. T. Wagner, *US Pat.*, 9,614.236 B2 (2017).
21. J. Yang, F.-B. Weng, C.-K. Cheng, and T.-W. Kuo, *US Pat. App.*, 2018/0166715 A1 (2018).
22. US DRIVE Fuel Cell Technical Team Roadmap: (https://energy.gov/eere/vehicles/downloads/us-drive-fuel-cell-technical-team-roadmap) Table P.9 on Page 29.
23. A. Kneer, J. Jankovic, D. Susac, A. Putz, N. Wagner, M. Sabharwal, and M. Secanell, *J. Electrochem. Soc.*, **165**, F3241 (2018).
24. Y. Yamashita, S. Itami, J. Takano, K. Kakinuma, H. Uchida, M. Watanabe, A. Iiyama, and M. Uchida, *J. Electrochem. Soc.*, **164**, F181 (2017).
25. M. Pourbaix, *Atlas of Electrochemical Equilibria in Aqueous Solutions* (National Association of Corrosion) (1974).